The RABiT-II DCA in the Rhesus Macaque Model

Authors: Royba, Ekaterina, Repin, Mikhail, Balajee, Adayabalam S., Shuryak, Igor, Pampou, Sergey, et al.

Source: Radiation Research, 196(5) : 501-509

Published By: Radiation Research Society

URL: https://doi.org/10.1667/RR15547.1

RADIATION RESEARCH **196**, 501–509 (2020)
0033-7587/20 $15.00

DOI: 10.1667/RR15547.1

The RABiT-II DCA in the Rhesus Macaque Model

Ekaterina Royba,[a,1,2] Mikhail Repin,[a] Adayabalam S. Balajee,[b] Igor Shuryak,[a] Sergey Pampou,[c] Charles Karan,[c] David J. Brenner[a] and Guy Garty[a]

[a] *Center for Radiological Research, Columbia University Irving Medical Center, New York, New York 10032;* [b] *Radiation Emergency Assistance Center/Training Site (REAC/TS), Cytogenetic Biodosimetry Laboratory (CBL), Oak Ridge Institute for Science and Education, Oak Ridge Associated Universities, Oak Ridge, Tennessee 37830; and* [c] *JP Sulzberger Columbia Genome Center, High-Throughput Screening Center, New York, New York 10032*

Royba, E., Repin, M., Balajee, A. S., Shuryak, I., Pampou, S., Karan, C., Brenner, D. J. and Garty, G. The RABiT-II DCA in the Rhesus Macaque Model. *Radiat. Res.* 196, 501–509 (2020).

An automated platform for cytogenetic biodosimetry, the "Rapid Automated Biodosimetry Tool II (RABiT-II)," adapts the dicentric chromosome assay (DCA) for high-throughput mass-screening of the population after a large-scale radiological event. To validate this test, the U.S. Federal Drug Administration (FDA) recommends demonstrating that the high-throughput biodosimetric assay in question correctly reports the dose in an *in vivo* model. Here we describe the use of rhesus macaques (*Macaca mulatta*) to augment human studies and validate the accuracy of the high-throughput version of the DCA. To perform analysis, we developed the 17/22-mer peptide nucleic acid (PNA) probes that bind to the rhesus macaque's centromeres. To our knowledge, these are the first custom PNA probes with high specificity that can be used for chromosome analysis in *M. mulatta*. The accuracy of fully-automated chromosome analysis was improved by optimizing a low-temperature telomere PNA FISH staining in multiwell plates and adding the telomere detection feature to our custom chromosome detection software, FluorQuant-Dic V4. The dicentric frequencies estimated from *in vitro* irradiated rhesus macaque samples were compared to human blood samples of individuals subjected to the same *ex vivo* irradiation conditions. The results of the RABiT-II DCA analysis suggest that, in the lymphocyte system, the dose responses to gamma radiation in the rhesus macaques were similar to those in humans, with small but statistically significant differences between these two model systems.

INTRODUCTION

The dicentric chromosome assay (DCA) is an established method of measuring radiation exposure and is considered by the International Organization for Standardization (ISO), International Atomic Energy Agency (IAEA) and U.S. Food and Drug Administration (FDA) to be the gold standard for biological biodosimetry (*1–4*). However, this assay is not very practical for mass screening, as it has a low throughput and is restricted to a certain time window for application (*5*). Recently, we achieved a high-throughput version of the DCA by miniaturization and parallelization of all procedures performed in multiwell plates by an automated robotic device, the Rapid Automated Biodosimetry Tool II (RABiT-II) (*6*). The next logical step, recommended by the FDA for the development of the RABiT-II DCA, is to ensure that this high-throughput assay correctly reports the dose for both *in vitro* and *in vivo* irradiated blood samples.

In vivo human studies are primarily limited to radiotherapy patients who have received fractionated doses, which often fail to cover doses of interest for dosimetry and do not necessarily mimic relevant exposure situations. Moreover, the blood samples from these patients may provide uncertainties in the dicentric rates because the lymphocytes are likely to get damaged due to the disease, or chemotherapy, in addition to the radiation treatment plans (*7*). When human validation studies are not possible, the FDA guidelines recommend using an appropriate animal model for assessment of the biodosimetry device performance (*8*). Successful extrapolation of the data from experimental animals to humans can be used to bridge the results of the assay from clinical doses to more realistic exposure scenarios (*9*).

Most information on aberration frequency *in vitro* versus *in vitro* irradiated blood has been obtained from animal studies (*10–13*). However, not all results derived using experimental animals are well applicable to humans. In some species, the dicentric yields were found to be related to the effective chromosome arm number in a way that a human male with an effective arm number of 81 has twice as many dicentrics as a mouse with the arm number 40 (*14*). In contrast, in the rabbit model, the dicentric yields were

Editor's note. The online version of this article (DOI: https://doi.org/10.1667/RR15547.1) contains supplementary information that is available to all authorized users.

[1] Address for correspondence: Center for Radiological Research, Columbia University Irving Medical Center, VC11-230, 630 West 168th Street, New York, NY 10032; email: er2889@cumc.columbia.edu.

[2] Scholar-in-Training, Radiation Research Society.

TABLE 1
The Nucleotide Sequences of the PNA Probes Used in this Study

Probe[a]	Probe sequence (N to C terminus)
M. mulatta test probe 1 (*pMm1*)	[FAM] - N'-ACTTCTTTGTGTTCTGT-C'
M. mulatta test probe 2 (*pMm2*)	[FAM] - N'-TCACAGAGTTACAGCTT-C'
M. mulatta test probe 3 (*pMm3*)	[FAM] - N'-GAATTCATCTCACAGAGTTACA-C'
H. sapiens custom centromere CENP-B probe	[FAM] - N'-ATTCGTTGGAAACGGGA-C'
C-rich telomere (TelC) probe	[Cy3] - N'-CCCTAACCCTAACCCTAA-C'
G-rich telomere (TelG) probe	[Cy3] - N'-TTAGGGTTAGGGTTAGGG-C'

[a] *pMm* = PNA probes derived from centromeric DNA repeats *Macaca mulatta* (*Mm)* and the number assigned for each probe.

less than half of those in humans, even though the arm numbers were almost comparable (*13*). Moreover, not all mammalian species are appropriate for testing an automated version of the DCA, as their chromosomes, with different morphology from those of humans, will be outside of the detection range of the custom software. This makes certain animal studies of limited utility for further validation of the RABiT-II DCA.

Rhesus macaques (*Macaca mulatta*), the most widely used non-human primate (NHP) species, have been recommended as a human substitute for various research applications (*15*), including practical biodosimetry (*16*). The manual DCA works just as well on the NHP model as on humans and has already demonstrated agreement with humans in the frequency of both stable (translocations) (*12*) and unstable (dicentric) (*13*) aberrations after irradiation. Concerning chromosomal size and morphology, in both species, the majority of chromosomes are bi-armed with almost equal numbers of effective chromosomal arms (84/83 vs. 82/81 for female/male rhesus macaques vs. humans, respectively) (*14, 17*). Remarkable genetic similarity (*18, 19*) and similar cell cycle kinetics of cultured primate lymphocytes to that in man (*13*) minimizes the impact of confounding factors [e.g., chromatin state and DNA repair pathway choice (*20, 21*)] that may influence radiosensitivity and the yield of dicentrics, reinforcing the suitability of this model for further validation of the high-throughput DCA.

The peptide nucleic acid (PNA) fluorescent *in situ* hybridization technique has radically improved chromosome aberration scoring (*22, 23*). Based on its ability to cover the alpha satellite sequences flanking the centromeres, PNA probes are an excellent tool for the automated discrimination between normal (one centromere) and aberrant (multiple centromere) chromosomes. However, as was shown in other primate species (*24*), the commercially available PNA probes, suitable for detection of human centromeres, do not hybridize to the rhesus macaque's centromeres. Therefore, prior to analysis, it was necessary to generate custom centromere probes for the detection of radiation damage in the rhesus macaques. We constructed PNA probes that allowed us to perform the DCA on the rhesus macaques using the automated RABIT-II system. To improve quality of automated chromosome analysis, we optimized our non-classical (37°C) PNA FISH staining (*6*) using both centromere and telomere probes, and updated our custom software to score entities with excess telomeres as chromosome clusters as opposed to true multicentric chromosomes. These improvements enabled automated comparison of the radiation responses of rhesus macaque blood samples to that of human blood samples subjected to the same *ex vivo* irradiation conditions, to establish equivalence between two species.

MATERIALS AND METHODS

Unless otherwise noted, all reagents and plasticware were purchased from Thermo Fisher Scientific™ Inc. (Waltham, MA).

Sequence Alignments and Probe Design

The PNA probes used in this study are listed in Table 1. The rhesus macaque centromere probes were designed using a 343-bp-long fragment of *M. mulatta* highly repeated DNA (PubMed nucleotide database, gene bank accession X04006.1, p Rh2 27). All sequence alignments were performed using A Plasmid Editor (ApE) software. Properties of the candidate oligomers (purine nucleotide composition, binding specificity and cross dimers) were analyzed using the PNABio tool (https://www.pnabio.com/support/PNA_Tool.htm) and Oli2go oligonucleotide design tool (http://oli2go.ait.ac.at/). Refined oligonucleotides were synthesized by Panagene (Daejeon, South Korea). The centromere PNA probes for human chromosomes and telomere PNA probes were ordered from a licensed Panagene distributor (PNA Bio Inc., Newbury Park, CA). All probes were received in lyophilized form and dissolved in formamide to a final concentration of 10 μ*M* (50 μg/ml). The aliquots were stored at –20°C in the dark.

Blood Samples

Animal blood samples (from 5 healthy males and 5 healthy females) were purchased from AlphaGenesis®, Inc. (Yemassee, SC), shipped at 20 ± 2°C to Columbia University (New York, NY), and processed immediately on arrival (within 24 h of blood draw). Human blood samples (from 5 healthy male and 5 female donors) were collected under Columbia University Institutional Review Board Protocol no. AAAR0643. After informed consent, the blood was drawn by venipuncture into BD Vacutainer™ plastic blood collection tubes with lithium heparin anticoagulant and processed immediately.

Irradiation

The blood aliquots were pipetted into 2D-barcoded tubes (Matrix Storage Tubes) and transported to a Gammacell®-40 ^{137}cesium (^{137}Cs) irradiator (Atomic Energy of Canada Ltd., Chalk River, Canada). The tubes were γ-ray irradiated (^{137}Cs) at 0, 2, 4, 6, 8 and 10 Gy at a dose rate of 0.73 Gy/min (measured at the height of 2 mm in the chamber). Annual calibration of the Gammacell-40 is performed by the chief

medical physicist at Columbia University Irving Medical Center's Department of Radiation Oncology, using thermoluminescent dosimeters (TLDs).

RABiT-II Automated Dicentric Assay

After irradiation, human blood samples were processed automatically using the RABiT-II DCA, as described elsewhere (*6*). Several modifications to this protocol were applied for culturing the rhesus macaque whole blood samples. For lymphocyte activation and expansion, RPMI-1640 medium (Mediatech Inc., Herndon, VA), supplemented with 20% heat-inactivated fetal bovine serum (FBS; HyClone™, Logan, UT) and 25 μg/ml of the mitogen concanavalin A (Sigma-Aldrich® LLC, St. Louis, MO) was used. After 44 h in culture, 0.1 μg/ml colcemid (Sigma-Aldrich) was dispensed into the multiwell plates. After a further 4 h incubation, cells were harvested, swollen in a hypotonic solution (0.075 *M* KCl), then fixed using a 3:1 methanol:acetic acid fixative. Chromosomes were released from mitotic nuclei and stained in multiwell plates using PNA FISH. Before staining, samples were blocked with 200 μl of 1% bovine serum albumin (BSA; Sigma-Aldrich) in PBS for 30 min at room temperature. Then, BSA was replaced with 200 μl of hybridization cocktail consisting of 90% formamide, 2× saline sodium citrate buffer [0.33 *M* sodium chloride in a 0.03 *M* sodium citrate buffer (pH 7.0)], 0.25 μg/ml of centromere PNA probe, and 0.05 μg/ml of telomere TelG probe. Hybridization was performed for 3 h at 37°C. After staining, 200 μl of PBS containing 1.5 μg/ml 4′,6-diamidino-2-phenylindole (DAPI) was dispensed in each well for counterstaining. After 10 min, 400 μl of staining mixture (PNAs and DAPI) was aspirated, the plates were then washed two times with 200 μl of PBS and imaged.

Image Acquisition and Analysis

Image acquisition was performed using the RABiT-II plate imager, a BioTek® Cytation 1 Cell Imaging Multi-Mode Reader (Winooski, VT), with low magnification (20× objective). From each well, a total of 450 image sets (size 380 × 280 μm per image, 1,152 × 832 pixels, 16 bit) from DAPI (blue), FITC (green), and RFP (red) channels were obtained and stored in an image gallery. Upon completion of the acquisition, the images were automatically analyzed for the presence of normal and aberrant chromosomes using our home-written software, FluorQuantDic V4 (*6*). Individual chromosomes were identified in the DAPI channel and only those falling within acceptable morphology were scored for bright foci in the corresponding region of the GFP (centromere) and RFP (telomere) images. Chromosomes with telomere spots more than 5 pixels from the edge of the chromosome were rejected. The software classified validated chromosomes as acentric, monocentric, dicentric, or multicentric chromosomes based on the number of detected centromere spots.

Dose-Response Curves and Statistical Analysis

Dose-response calibration curves were constructed using DoseEstimate software version 5.2 (*25*). The coefficients of the fitted curves were derived for collectively pooled individuals (2 replicates per animal/donor). For statistical analysis, we performed a customized fit to the dicentric fraction data using a linear-quadratic (LQ) dose dependence, with binomially-distributed errors. This was done using Maple 2018 software (MapleSoft, Waterloo, Canada) by the maximum likelihood of pooled data for each species separately. Additionally, to examine variability in radiation responses between macaques and humans, we performed mixed-effects modeling using logistic regression in the lme4 R package. Equation (1), below, was used for the dicentric probability (P = number of dicentrics/number of scored chromosomes), where b is the background parameter, α and β are standard LQ dose-response parameters and D is the dose:

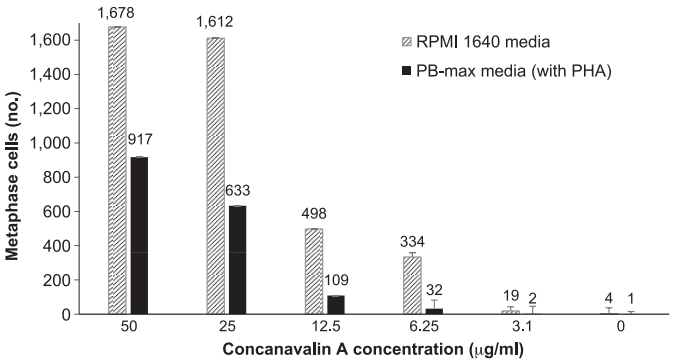

FIG. 1. Mitogen-induced rhesus macaque lymphocyte proliferation. The yields were examined after 48 h incubation with concanavalin A alone or in combination with PHA. Quantification data represent a total number of metaphase cells scored in one well. Error bars reveal standard error of the mean (n = 3) and represent the mean of three independent experiments.

$$P = 1 - exp\left[-\left(b + \alpha D + \beta D^2\right)\right] \quad (1)$$

The $1 - exp$ structure was used to prevent P from becoming >1 at high doses, thus allowing it to be treated as a probability rather than a yield. At relatively small P values (<0.12) this adjustment is not very important numerically but facilitates the analysis. Comparisons between actual and reconstructed doses were performed by solving Eq. (1) for D, using P values from the measured human data as the input. This produced two sets of reconstructions: using macaque parameters and using human parameters. A real solution for D becomes complex and cannot be calculated if $P < b$, so in those instances D was set to zero. A paired t test was used to compare dose reconstructions based on human dicentrics data, but using best-fit LQ model parameters for either macaques or humans.

RESULTS

Optimization of the RABiT-II DCA Protocol for Rhesus Macaques

Compared to human lymphocytes, the PB-MAX karyotyping media containing phytohemagglutinin (PHA) as a mitogen had minimal effectiveness to trigger the proliferation of the rhesus macaque's lymphocytes (*26*). To increase the yields of rhesus chromosomes scored using RABiT-II DCA, we tested several culture media and mitogen combinations (Fig. 1). The effect of mitogens was assessed by manual scoring of mitotic indexes throughout the observation of images captured on a BioTek plate imager. The highest mitotic index was registered in RPMI-1640 media containing 20% FBS supplemented with 25 to 50 μg/ml concanavalin A (Fig. 1). Thus, the rhesus experiments in this study were performed with a 25 μg/ml concanavalin A.

Design of the Centromere PNA Probe for Use in Rhesus Macaque DCA and Optimization of Centromere-Telomere PNA FISH Staining at 37°C

Preliminary staining tests revealed that the commercial human centromere PNA probe does not hybridize to rhesus macaque centromeres. To our knowledge, alternative PNA

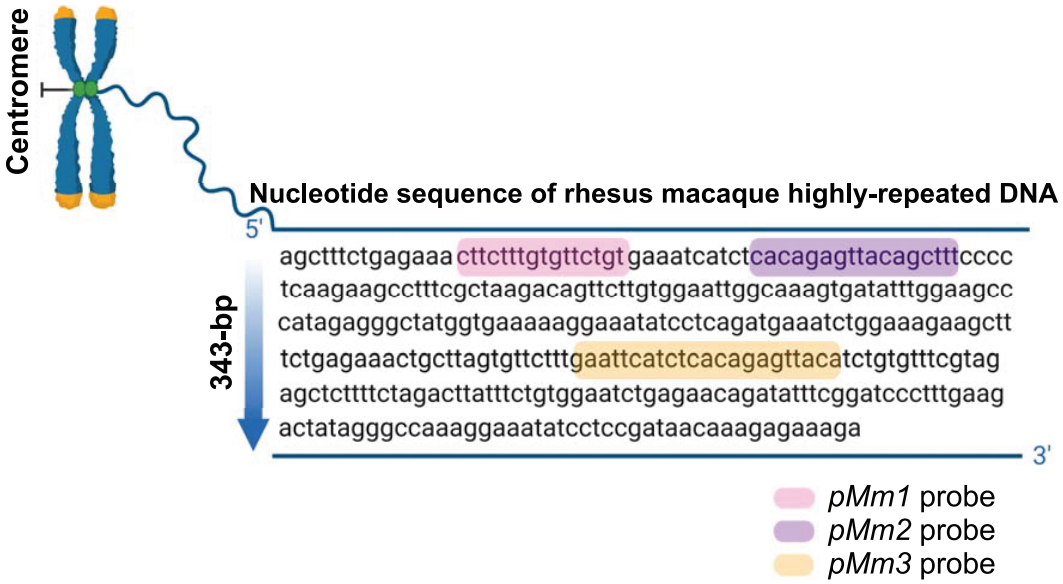

FIG. 2. The nucleotide sequence of the 343-base-pair highly repeated fragment of *M. mulatta* DNA and locations of the centromere PNA probes designed for this study. The format of presentation is such that the target sequences for hybridization of the *pMm1*, *pMm2* and *pMm3* PNA probes are highlighted by different colors (pink, purple and yellow, respectively).

probes for staining of *M. mulatta* centromeres are not available and were not previously reported by other researchers. To generate centromere PNA probes for the dicentric analysis of rhesus macaque lymphocytes, we analyzed the nucleotide sequence of the 343-base-pair highly repeated fragment of the rhesus macaque DNA and selected 15 candidate regions with a length not longer than 22-bp each. Subsequently, the chemical properties of these oligonucleotides were analyzed to select a total of 3 candidate PNA probes (Fig. 2 and Table 2). These probes were ordered from a commercial distributor. The efficiency of the probe hybridization to the rhesus macaque centromeres and the stability of the duplexes was analyzed at 75°C (classical PNA FISH) and 37°C (the RABiT-II DCA) hybridization. We found that at 37°C, the *pMm1* PNA probe did not produce any fluorescent signal, whereas the *pMm2* and the *pMm3* PNA probes have sufficiently stained the rhesus centromeres. In this work, for staining the rhesus macaque centromeres, we used the 17-mer *pMm2* PNA probe (Fig. 2).

For optimization of telomere staining without heat denaturation (37°C), we tested both the C-rich and the G-rich telomere probes. We observed a strong dependence of telomere probe hybridization performance on the concentration of formamide in the hybridization mixture (Fig. 3). Specifically, the TelC probe did not hybridize at 90% formamide, which can be due to probe detachment during washing (*27*). In contrast, the TelG probe demonstrated excellent hybridization at 37°C in 80% to 90% formamide for both species (humans and rhesus macaques) (Fig. 4). The TelG probe was chosen for further experiments with both species.

Comparison of Rhesus Macaque and Human Responses to Gamma Radiation

After culturing and staining were optimized for both species, the number of chromosomes and yields of dicentrics in *ex vivo* irradiated human and animal blood samples were automatically scored using the FluorQuantDic V4 software. The raw results of scoring for macaques and humans are given in Supplementary Tables S1 and S2 (https://doi.org/10.1667/RR15547.1.S1), respectively. The average fraction of dicentrics is shown in Table 3. To characterize statistical variation attributable to both model systems, we used LQ and logistic regressions, including an

TABLE 2
Selected Properties of the Designed Rhesus Macaque Centromere Probes

Probe[a]	Probe size	Probe location on alpha-satellite	Hybridization temperature	G/C content
pMm1	17mer	14 to 30bp	75°C	35.30%
pMm2	17mer	40 to 56bp	37°C and 75°C	41.20%
pMm3	22mer	203-225 bp	37°C and 75°C	36.36%

[a] *pMm* = PNA probes derived from centromeric DNA repeats *Macaca mulatta* (*Mm)* and the number assigned for each probe.

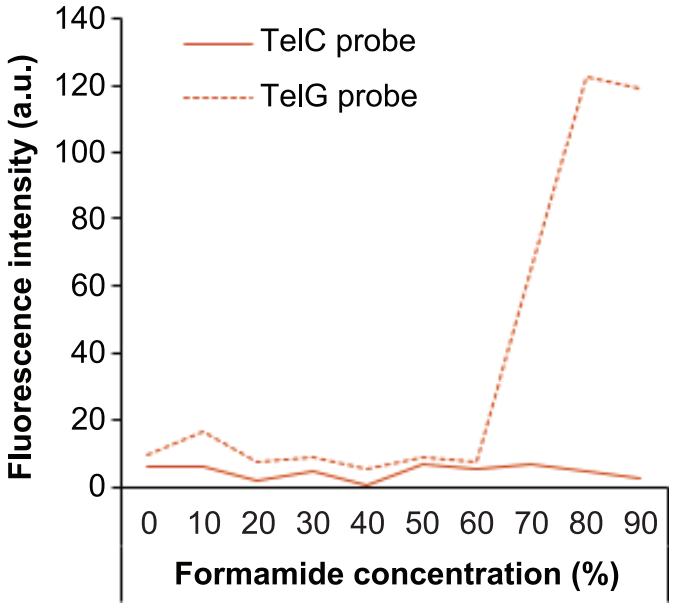

FIG. 3. Non-heat hybridization performance of the TelG and the TelC probes in formamide. Various formamide concentrations were used instead of high temperatures to adjust the access of the probes to the target telomere repeats on the rhesus macaque and human chromosomes. An optimal range of formamide concentration of binding of the TelG probe was 80–90%.

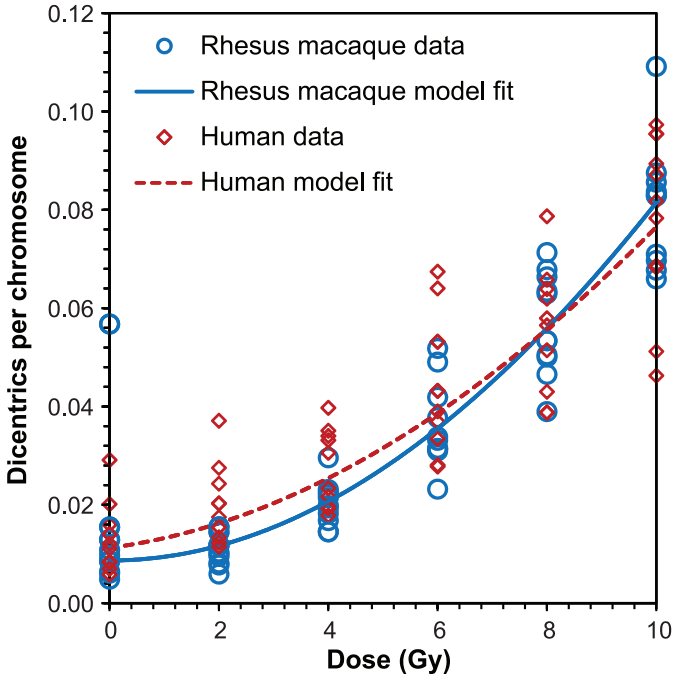

FIG. 5. Linear-quadratic fits for the rhesus macaque and human data. Best fits for macaques or humans are represented by blue or red solid lines, respectively; the individual results are indicated by blue circles or red diamond dots (for macaques or humans, respectively).

assessment of inter-donor variability in the dose-response parameters.

The customized LQ model (Eq. 1) fits are shown in Fig. 5. These data summarize the fraction of the dicentrics in each sample obtained from 10 animals and 10 human individuals (two technical repeats for each dose). Macaque best-fit parameters were: $b = 8.71 \times 10^{-3}$, $\alpha = 0$ Gy^{-1} and $\beta = 7.62 \times 10^{-4}$ Gy^{-2}. Human best-fit parameters were: $b = 1.13 \times 10^{-2}$, $\alpha = 1.46 \times 10^{-3}$ Gy^{-1} and $\beta = 5.36 \times 10^{-4}$ Gy^{-2}. Table 4 shows the uncertainties for each model parameter,

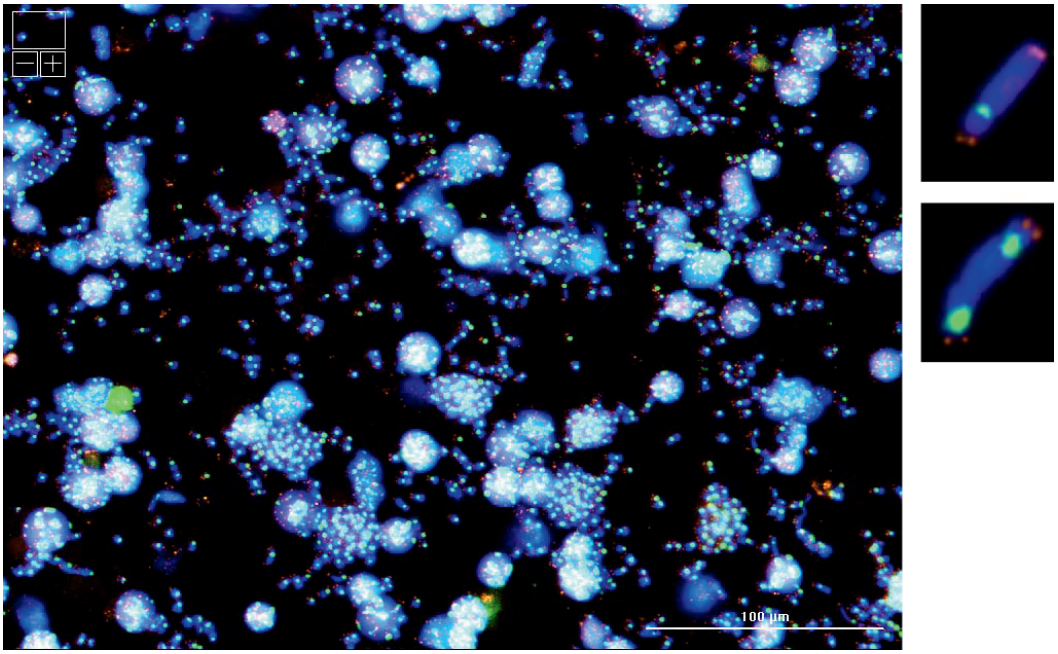

FIG. 4. Representative images of the rhesus macaque isolated chromosomes (left side image) and enlarged images of normal and dicentric chromosomes acquired using a plate imager, 20× magnification (see Materials and Methods).

TABLE 3
Dicentric Chromosome Frequencies in Macaques and Human Samples Scored by the FluorQuantDic V4

Species	Dose (Gy)	Chromosomes	DCs	Yield ± standard error
M. mulatta	0.0	111,915	1,059	0.009 ± 0.000
	2.0	122,772	1,306	0.011 ± 0.000
	4.0	79,417	1,624	0.020 ± 0.001
	6.0	62,338	2,283	0.037 ± 0.001
	8.0	45,208	2,527	0.056 ± 0.001
	10.0	43,054	3,497	0.081 ± 0.001
H. sapiens	0.0	55,911	620	0.011 ± 0.000
	2.0	52,595	883	0.017 ± 0.001
	4.0	49,912	1,271	0.025 ± 0.001
	6.0	36,127	1,358	0.038 ± 0.001
	8.0	28,764	1,591	0.055 ± 0.001
	10.0	22,090	1,723	0.078 ± 0.002

Note. Data pooled from 10 animals/donors (Supplementary Tables S1 and S2; https://doi.org/10.1667/RR15547.1.S1). DCs = dicentric chromosomes.

calculated using profile likelihood. The 0 Gy data from animal 4 has an abnormally high probability of dicentrics, probably due to the low number of chromosomes (a total of 405) scored for this dose point (Supplementary Table S1; https://doi.org/10.1667/RR15547.1.S1). However, exclusion of this animal from the analysis had only small effects on model parameters (Table 4), probably because the ''weight'' of the outlier data at 0 Gy for animal 4 was very small due to the small number of scored chromosomes.

Graphs of dose reconstructions of human doses based on the human calibration curve ($R^2 = 0.8$) and the macaque calibration curve ($R^2 = 0.8$) are shown in Fig. 6. A paired *t* test, however, showed a significant difference between the dose reconstructions: those using human parameters were, on average, lower than those using macaque parameters (*P* value 1.85×10^{-6}, 95% CI: –0.59 to –0.26 Gy). Additional information on the inter-donor variability analysis performed without pooling the data is shown in the Supplementary Text, Figs. S1 and S2, and Tables S3 and S4 (https://doi.org/10.1667/RR15547.1.S1)

DISCUSSION

The RABiT-II is the fully-automated biodosimetry platform for high-throughput emergency screening of a large number of individuals exposed to an unknown level of ionizing radiation/s (*28*). Using this robotic system, we recently implemented the RABiT-II DCA (*6*) to score aberrant chromosomes in human blood automatically. The results of the RABiT-II DCA determine the dose absorbed by the whole body to detect significant radiation exposures during triage assessment. While no difference between *in vitro* and *in vivo* measurements of chromosomal aberrations is expected (*10–13*), the FDA requires this to be demonstrated for each specific assay prior to licensure. *In vivo* studies in humans using radiotherapy patients are a less suitable model for validation of the RABiT-II DCA since some treatment plans can elevate chromosome breakage, and the dicentric chromosomes can arise as a direct result of the previous therapies (*7*). Thus, the animal study using the rhesus macaque model has been performed instead.

TABLE 4
The Fit Parameters for the LQ Probability Model with Errors 95% Confidence Intervals (CIs) for Each Model Parameter Calculated Using Profile Likelihood

Model parameter	Human best-fit value	95% CIs		Monkey best-fit value	95% CIs		Monkey best-fit value, no animal 4	95% CIs	
b (background)	1.13E–02	1.05E–02	1.22E–02	8.71E–03	8.33E–03	9.11E–03	8.73E–03	8.34E–03	9.13E–03
Alpha (Gy^{-1})	1.46E–03	8.66E–04	2.06E–03	0	0	2.20E–05	0	0	2.20E–05
Beta (Gy^{-2})	5.36E–04	4.64E–04	6.11E–04	7.62E–04	7.44E–04	7.82E–04	7.79E–04	7.56E–04	7.98E–04

	Model parameter					
	b (background)		Alpha (Gy^{-1})		Beta (Gy^{-2})	
Human best-fit value	1.13E–02		1.46E–03		5.36E–04	
95% CIs	1.05E–02	1.22E–02	8.66E–04	2.06E–03	4.64E–04	6.11E–04
Monkey best-fit value	8.71E–03		0		7.62E–04	
95% CIs	8.33E–03	9.11E–03	0	2.20E–05	7.44E–04	7.82E–04
Monkey best-fit value, no animal 4	8.73E–03		0		7.79E–04	
95% CIs	8.34E–03	9.13E–03	0	2.20E–05	7.56E–04	7.98E–04

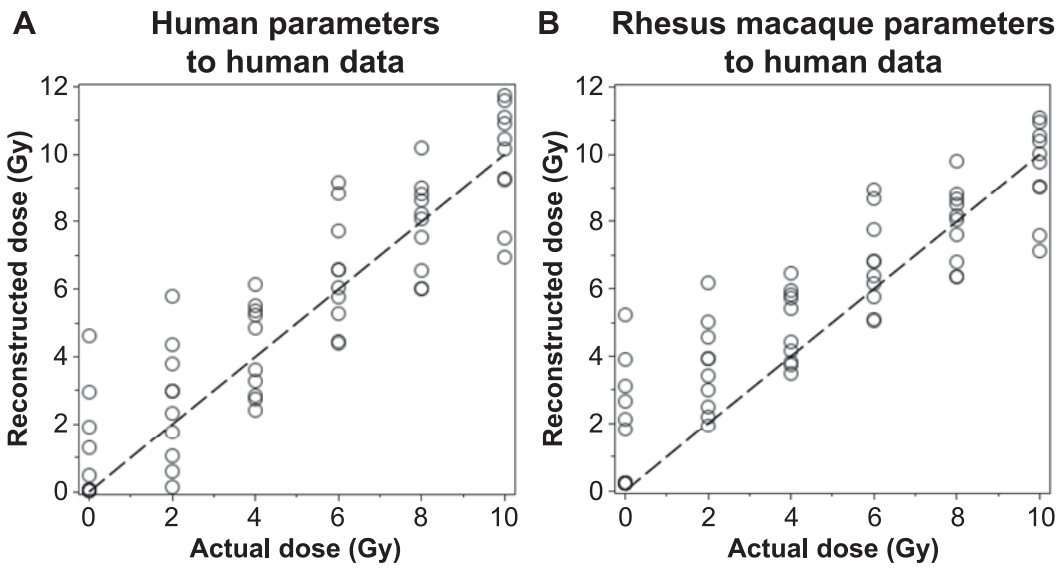

FIG. 6. Comparisons of actual vs. reconstructed doses: Panel A: Human parameters applied to human data. Panel B: Rhesus macaque parameters applied to human data. Dashed lines show a theoretically perfect 1:1 correlation.

Taking into account various factors operating during automated sample preparation, all essential experimental procedures and cytogenetic techniques that had been previously used for human samples were well applicable to the rhesus macaques. None of the technical issues, reported earlier, including difficulties with obtaining sufficient yields of mitotic cells or unsatisfactory quality of mitotic spreads, such as overlapping chromosomes in metaphase cells (*26, 29*), were observed in our established workflow. The quality of mitotic spreads is not an issue in the RABiT-II DCA since it extracts the chromosomes from metaphase cells and performs the analysis on isolated chromosomes; high mitotic yields were achieved in all experiments using concanavalin A. The culture conditions and fixation time of the blood cultures obtained from both species were in good agreement and were suitable for interspecies comparison of the dicentric yields.

The molecular target for binding of the commercial centromere PNA probe is the 17-mer centromere protein (CENP) B box sequence on the alpha satellite DNA. In humans, the alpha satellite DNA consists of tandem repeats of 171-bp-long monomer units (*30*). Our sequence alignment has revealed no identical 17-mer CENP-B box sequence on the rhesus macaque's alphoid DNA. The rhesus macaque satellite DNA was longer (343-bp long dimer), comprised of the two monomer units (172-bp and 171-bp) that are quite divergent from each other (*31*). Indeed, the consensus sequence of the rhesus macaque satellite is more than 98% homologous to baboons but is only partially homologous (less than 70%) to the most diverged alphoid sequence of humans (*31*). Therefore, to realize dicentric analysis for the rhesus macaques using PNA probes, we developed custom *M. mulatta* centromere probes. To our knowledge, these probes are the first reported probes that allow for performing dicentric analysis in rhesus macaques using PNA FISH staining.

The developed PNA probes enabled a fully-automated comparison of the dicentric chromosome rate of rhesus macaque to that of human blood samples that were subjected to the same irradiation conditions, mimicking acute whole-body exposure to gamma rays. It is noteworthy that dicentric yields in the lymphocytes of the rhesus macaques examined in this study were similar to that of humans (Fig. 5). These findings are in agreement with previously reported studies that used manual DCA (*13*) or other techniques for comparison of both species. Specifically, rhesus macaques and humans have shown similar changes in expression of the radiation response genes (*32*) and kinetics of H2AX phosphorylation in the sites of nascent DNA double-strand breaks (*33*).

More rigorous statistical analysis for the RABiT-II DCA has demonstrated that there are small differences in best-fit parameters between macaque and human dicentric yields, although inter-donor variability ranges were overlapping. Regression fits were used to reconstruct doses. Doses reconstructed using macaque parameters applied to human data were not dramatically different from those reconstructed using human parameters, although the difference between means did reach statistical significance. The dose reconstruction accuracies tended to be better at higher doses than at lower doses (Fig. 6) because of the curved shape of the dose response (Fig. 5): at lower doses, there are smaller differences with baseline values, magnifying the errors in dose reconstruction. In these circumstances, several factors determining these small statistical differences on the yields of dicentrics can be considered, but the actual cause needs to be clarified. We can assume that an automated DCA requires more samples to be analyzed to obtain more precise

statistical data. Alternatively, the chromosomal radiosensitivity can be essentially the same for animal and human cells (*13*) but can be modified by the efficacy of detection of DNA damage at lower doses or by the DNA repair mechanisms, which can differ between these two species (*14*). This remains to be elucidated by an appropriate statistical study in the future.

SUPPLEMENTARY INFORMATION

Supplementary Text. Assessment of Differences in Radiation Dose Response Between Species and Between Individuals Within Each Species by Logistic Regression. Effects on Dose Reconstruction.

Table S1. RABiT-II DCA yields after *in vitro* γ-ray irradiation of rhesus macaque blood samples derived from 10 healthy animals.

Table S2. The RABiT-II DCA yields after *in vitro* γ-ray irradiation of human blood samples derived from 10 healthy donors.

Table S3. Dose-response parameters and intercepts across animals 1–10.

Table S4. Dose-response parameters and intercepts across donors 1–10.

Fig. S1. Logistic regression fits for (panel A) rhesus macaque and (panel B) human data. Best fits are represented by the curves; samples by the symbols.

Fig. S2. Comparisons of actual vs. reconstructed doses. Panel A: Human parameters applied to human data. Panel B: Rhesus macaque parameters applied to human data. Dashed lines show a theoretically perfect 1:1 correlation.

ACKNOWLEDGMENTS

We thank Maria Taveras for blood collection. This work was supported by the National Institute of Allergy and Infectious Diseases, National Institutes of Health, (NIAID/NIH contract no. HHSN272201600040C).

Received: October 25, 2019; accepted: May 8, 2020; published online: October 6, 2020

REFERENCES

1. ISO 21243:2008. Radiation protection - Performance criteria for laboratories performing cytogenetic triage for assessment of mass casualties in radiological or nuclear emergencies - General principles and application to dicentric assay. Geneva: International Organization for Standardization; 2008–2009. (https://www.iso.org/standard/40088.html)
2. ISO 19238:2004. Radiation protection - Performance criteria for service laboratories performing biological dosimetry by cytogenesis. Geneva: International Organization for Standardization; 2004–2008. (https://www.iso.org/standard/33759.html)
3. Cytogenetic dosimetry: Applications in preparedness for and response to radiation emergencies. EPR-Biodosimetry. Vienna: International Atomic Energy Agency; 2011.
4. Radiation biodosimetry devices: Draft guidance for industry and Food and Drug Administration staff. Report no. UCM427866. Silver Spring, MD: U.S. Department of Health and Human Services, Food and Drug Administration Center for Devices and Radiological Health; 2014.
5. Sproull MT, Camphausen KA, Koblentz GD. Biodosimetry: A future tool for medical management of radiological emergencies. Heal Secur 2017; 15:599–610.
6. Royba E, Repin M, Pampou S, Karan C, Brenner DJ, Garty G. RABiT-II-DCA: A fully-automated dicentric chromosome assay in multiwell plates. Radiat Res 2019; 192:311–23.
7. Andersen M, Pedersen-Bjergaard J. Increased frequency of dicentric chromosomes in therapy-related MDS and AML compared to de novo disease is significantly related to previous treatment with alkylating agents and suggests a specific susceptibility to chromosome breakage at the centromere. Leukemia 2000; 14:105–11.
8. Radiation biodosimetry medical countermeasure devices guidance for industry and Food and Drug Administration staff. Silver Spring, MD: U.S. Department of Health and Human Services, Food and Drug Administration Center for Devices and Radiological Health; 2016.
9. Singh VK, Seed TM. A review of radiation countermeasures focusing on injury-specific medicinals and regulatory approval status: part I. Radiation sub-syndromes, animal models and FDA-approved countermeasures. Int J Radiat Biol 2017; 93:851–69.
10. Bajerska A, Liniecki J. The yield of chromosomal aberrations in rabbit lymphocytes after irradiation in vitro and in vivo. Mutat Res 1975; 27:271–84.
11. Darroudi F, Farooqi Z, Benova D, Natarajan AT. The mouse splenocyte assay, an in vivo/in vitro system for biological monitoring: studies with X-rays, fission neutrons and bleomycin. Mutat Res 1992; 272:237–48.
12. Lucas JN. Stability of the translocation frequency following whole-body irradiation measured in rhesus monkeys. Int J Radiat Biol 1996; 70:309–18.
13. Hirai M, Nakai S. Dicentric yields induced by gamma-radiation and chromosome arm number in primates. Mutat Res 1977; 43:147–57.
14. Van Buul PPW. A comparative study of the frequencies of radiation-induced chromosome aberrations in somatic and germ cells of the rhesus monkey (Macaca mulatta). Mutat Res 1976; 36:223–35.
15. Singh VK, Olabisi AO. Nonhuman primates as models for the discovery and development of radiation countermeasures. Expert Opin Drug Discov 2017; 12:695–709.
16. Park JG, Paul S, Briones N, Zeng J, Gillis K, Wallstrom G, et al. Developing human radiation biodosimetry models: Testing cross-species conversion approaches using an ex vivo model system. Radiat Res 2017; 187:708–21.
17. Pellicciari C, Formenti D, Redi CA, Manfredi MG, Romanini. DNA content variability in primates. J Hum Evol 1982; 11:131–41.
18. Soares MBM, Armada JLA, da Silva VF, Seuanez HN. Standardization of the karyotype of the Rhesus monkey, Macaca mulatta, and Interspecific homologies with human chromosomes. J Hum Evol 1982; 11:291–6.
19. Gibbs RA, Worley KC, Kehrer-Sawatzki H, Cooper DN. The sequencing of the rhesus macaque genome and its comparison with the genome sequences of human and chimpanzee. In: Encyclopedia of Life Sciences. Chichester, UK: John Wiley & Sons, Ltd; 2008.
20. Hustedt N, Durocher D. The control of DNA repair by the cell cycle. Nat Cell Biol 2017; 19:1–9.
21. Chao HX, Poovey CE, Privette AA, Grant GD, Chao HY, Cook JG, et al. Orchestration of DNA damage checkpoint dynamics across the human cell cycle. Cell Syst 2017; 5:445–49.e5.
22. Shi L, Fujioka K, Sun J, Kinomura A, Inaba T, Ikura T, et al. A modified system for analyzing ionizing radiation-induced chromosome abnormalities. Radiat Res 2012; 177:533–8.
23. George K, Willingham V, Cucinotta FA. Stability of chromosome aberrations in the blood lymphocytes of astronauts measured after

space flight by FISH chromosome painting. Radiat Res 2005; 164:474–80.

24. Haaf T, Mater AG, Wienberg J, Ward DC. Presence and abundance of CENP-B box sequences in great ape subsets of primate-specific alpha-satellite DNA. J Mol Evol 1995; 41:487–91.

25. Ainsbury EA, Lloyd DC. Dose estimation software for radiation biodosimetry. Health Phys 2010; 98:290–5.

26. Loftin KC, Levy BM. A micro-culture technique for the mitogen stimulation of lymphocytes from Macaca mulatta (rhesus) and Macaca fascicularis (cynomolgus). Primates 1983; 24:118–26.

27. Carbonari M, Cibati M, Sette N, Catizone A, Fiorilli M. Measurement of telomere length using PNA probe by cytometry. Methods Cell Biol 2011; 103:189–202.

28. Garty G, Bigelow AW, Repin M, Turner HC, Bian D, Balajee AS, et al. An automated imaging system for radiation biodosimetry. Microsc Res Tech 2015; 78:587–98.

29. Petibone DM, Morris SM, Hotchkiss CE, Mattison DR, Tucker JD. Technique for culturing Macaca mulatta peripheral blood lymphocytes for fluorescence in situ hybridization of whole chromosome paints. Mutat Res 2008; 653:76–81.

30. Giunta S, Funabiki H. Integrity of the human centromere DNA repeats is protected by CENP-A, CENP-C, and CENP-T. Proc Natl Acad Sci U S A 2017; 114:1928–33.

31. Pike LM, Carlisle A, Newell C, Hong SB, Musich PR. Sequence and evolution of rhesus monkey alphoid DNA. J Mol Evol 1986; 23:127–37.

32. Iversen ES, McCarthy JM, Bell Burdett K, Lipton G, Phillips G, Dressman H, et al. Bridging the gaps: using an NHP model to predict single dose radiation absorption in humans. Int J Radiat Biol 2020; 96:47–56.

33. Redon CE, Nakamura AJ, Gouliaeva K, Rahman A, Blakely WF, Bonner WM. The use of gamma-H2AX as a biodosimeter for total-body radiation exposure in non-human primates. PLoS One 2010; 5:e15544.